PNAS RESEARCH ARTICLE | PHYSIOLOGY

Evidence supporting the MICU1 occlusion mechanism and against the potentiation model in the mitochondrial calcium uniporter complex

Chen-Wei Tsai[a,1], Tsung-Yun Liu[a,1], Fan-Yi Chao[a], Yung-Chi Tu[a], Madison X. Rodriguez[a], Anna M. Van Keuren[a], Zhiwei Ma[b], John Bankston[a], and Ming-Feng Tsai[a,2]

Edited by Richard Lewis, Stanford University, Stanford, CA; received October 17, 2022; accepted March 3, 2023

The mitochondrial calcium uniporter is a Ca^{2+} channel that imports cytoplasmic Ca^{2+} into the mitochondrial matrix to regulate cell bioenergetics, intracellular Ca^{2+} signaling, and apoptosis. The uniporter contains the pore-forming MCU subunit, an auxiliary EMRE protein, and the regulatory MICU1/MICU2 subunits. Structural and biochemical studies have suggested that MICU1 gates MCU by blocking/unblocking the pore. However, mitoplast patch-clamp experiments argue that MICU1 does not block, but instead potentiates MCU via allosteric mechanisms. Here, we address this direct clash of the proposed MICU1 function. Supporting the MICU1-occlusion mechanism, patch-clamp demonstrates that purified MICU1 strongly suppresses MCU Ca^{2+} currents, and this inhibition is abolished by mutating the MCU-interacting K126 residue. Moreover, a membrane-depolarization assay shows that MICU1 prevents MCU-mediated Na^{+} flux into intact mitochondria under Ca^{2+}-free conditions. Examining the observations underlying the potentiation model, we found that MICU1 occlusion was not detected in mitoplasts not because MICU1 cannot block, but because MICU1 dissociates from the uniporter complex. Furthermore, MICU1 depletion reduces uniporter transport not because MICU1 can potentiate MCU, but because EMRE is down-regulated. These results firmly establish the molecular mechanisms underlying the physiologically crucial process of uniporter regulation by MICU1.

calcium channels | intracellular calcium signaling | mitochondrial physiology | organellar channels

Significance

The uniporter is crucial for normal physiology and its malfunction has been implicated in neurodegenerative diseases, tissue injuries following heart attacks, and cancer, among others. This Ca^{2+} channel is activated by cytoplasmic Ca^{2+} signals, but the mechanisms of Ca^{2+} activation are under debate. An "occlusion model" argues that Ca^{2+} binding to an MICU1 subunit releases MICU1 occlusion of the Ca^{2+} pathway to open the uniporter. However, a "potentiation model" proposes that MICU1 does not block but enhances uniporter function. This study provides evidence to support MICU1 occlusion and offers alternative interpretations for the observations underlying the potentiation model. These results bring the field closer to a unifying molecular understanding of the interplay between the uniporter and intracellular Ca^{2+} signaling.

The mitochondrial Ca^{2+} uniporter (hereafter referred to as the "uniporter") is a multisubunit Ca^{2+} channel complex that mediates mitochondrial Ca^{2+} uptake across the inner mitochondrial membrane (IMM). Its transmembrane (TM) region contains the MCU subunit that forms a tetrameric Ca^{2+} pore (1–6), and the EMRE protein that binds to MCU to stabilize the pore's conducting conformation (7–10). In the intermembrane space (IMS), the MICU1 subunit forms a homodimer or heterodimerizes with MICU2 (the neuron-specific MICU3 is not discussed here) to regulate uniporter activity (11–14). This MICU1 regulation is important for physiology, as MICU1 mutations have been linked to severe neuromuscular disorders in humans (15, 16), and MICU1 knockout (KO) is perinatally lethal in mice (17). The exact regulatory function and mechanisms of MICU1, however, are currently under debate.

Biochemical and functional studies (9, 18, 19) have established an "occlusion" mechanism that in resting cytoplasmic [Ca^{2+}] (~100 nM), MICU1 binds to the Ca^{2+}-coordinating Asp ring at the cytoplasmic entrance of the MCU pore to shut the channel (Fig. 1*A*). When intracellular Ca^{2+} signals raise [Ca^{2+}] around the uniporter, Ca^{2+} binding to the four EF hands in the MICU1-containing dimer causes MICU1 separation from the pore to enable Ca^{2+} permeation (Fig. 1*A*). Of note, EMRE contacts MICU1 via electrostatic interactions in a Ca^{2+}-independent manner so as to maintain MICU1 in the uniporter complex when the MCU–MICU1 interaction is disrupted by Ca^{2+} elevation (Fig. 1*A*). The key observations for this mechanism include the following: First, coimmunoprecipitation shows that MCU can bind to MICU1 without EMRE, and that this interaction is abolished by Ala substitution in the Asp ring (D261A) (18); second, a quantitative $^{45}Ca^{2+}$ flux assay shows that wild-type (WT) MCU exhibits virtually no transport activity in resting [Ca^{2+}], but introducing the D261A mutation to MCU or removing MICU1 both lead to robust mitochondrial Ca^{2+} uptake under the same low Ca^{2+} condition (18); and third, MICU1 competes with a uniporter inhibitor Ru360 (19), which is known to bind D261. Recent cryo-electron microscope work reveals the structural basis of the occlusion mechanism (20–22). In low [Ca^{2+}], MICU1 uses conserved Arg/Lys residues to contact MCU's D261 ring to block the channel (Fig. 1*B*). Ca^{2+} binding to the MICU1 dimer induces conformational changes that disrupt the MCU–MICU1 electrostatic

Author contributions: C.-W.T. and M.-F.T. designed research; C.-W.T., T.-Y.L., F.-Y.C., Y.-C.T., M.X.R., A.M.V.K., Z.M., and M.-F.T. performed research; J.B. contributed analytic tools; C.-W.T., T.-Y.L., F.-Y.C., and M.-F.T. analyzed data; and M.-F.T. wrote the paper.

The authors declare no competing interest.

This article is a PNAS Direct Submission.

[1]C.-W.T. and T.-Y.L. contributed equally to this work.

[2]To whom correspondence may be addressed. Email: ming-feng.tsai@cuanschutz.edu.

This article contains supporting information online at https://www.pnas.org/lookup/suppl/doi:10.1073/pnas.2217665120/-/DCSupplemental.

Published April 10, 2023.

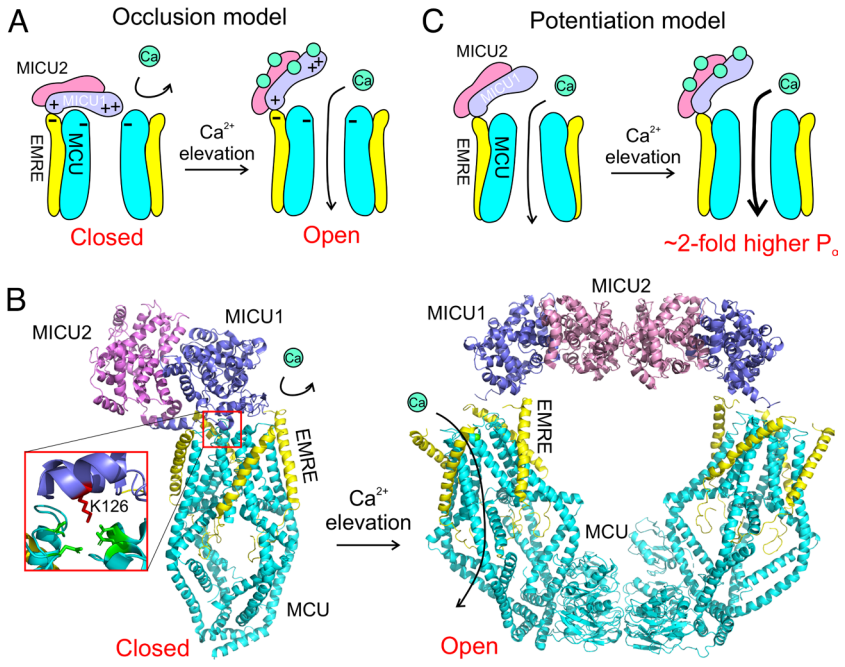

Fig. 1. Two models for Ca^{2+}-dependent gating of the uniporter. (*A*) The occlusion model. The cartoon illustrates that MICU1 interacts with both EMRE and MCU via electrostatic interactions in low Ca^{2+}. In high Ca^{2+}, the MCU–MICU1 interaction is disrupted so that Ca^{2+} can pass the pore, but the EMRE–MICU1 interaction remains intact to keep MICU1 associated within the uniporter complex. (*B*) Uniporter holocomplex structures in low (PDB: 6WDN) or high Ca^{2+} (6WDO). These structures recapitulate the key features in the occlusion model that MICU1 blocks MCU in low Ca^{2+} (*Left*) but swings away to open the pore in high Ca^{2+} (*Right*). The *Inset* highlights MICU1's K126 residue, which interacts with the D261 ring (green residues) to block the Ca^{2+} pathway. (*C*) The potentiation model. This model proposes that MICU1 does not block, but functions to increase MCU open probability via EMRE-dependent allosteric mechanisms.

interactions to open the pore (Fig. 1*B*). Subsequent functional studies further show that mutations of the MCU-interacting Arg/Lys eliminate MICU1 block (22).

The occlusion model, however, cannot explain multiple results obtained via patch-clamp recording of mitoplasts (a submitochondrial vesicle rid of the outer membrane). In a landmark study that demonstrates conclusively that the uniporter is a bona fide Ca^{2+} channel (23), it was observed that the uniporter, similar to many other Ca^{2+} channels (24, 25), can conduct Na^{+} in 0 Ca^{2+}. This observation, however, apparently contradicts the idea that MICU1 physically occludes the MCU pore under low-Ca^{2+} conditions. Expanding on this initial finding, a more recent mitoplast patch-clamp work (26) proposes that MICU1 never blocks, and further puts forth an alternative "potentiation model" (Fig. 1*C*). Based on the finding that MICU1-KO reduces uniporter Ca^{2+} currents by ~50% in >30 μM Ca^{2+}, it was argued that MICU1's real function is to potentiate the uniporter in elevated [Ca^{2+}]. Here, our goal is to understand why extensive work from multiple laboratories over the last two decades produce two entirely opposite models underlying Ca^{2+}-dependent, MICU1-mediated uniporter gating.

Results

Purified MICU1 Blocks MCU Ca^{2+} Currents. The most critical difference between the occlusion and potentiation models is that the former requires the presence of a MICU1-mediated, blocked state, while the latter demands that MICU1 block does not exist. Thus, the key to determine which model is correct is to examine whether there is a blocked state. We thus test whether purified MICU1 can block MCU Ca^{2+} currents, analogous to classical K^{+} channel work (27, 28) showing that purified neurotoxins (e.g., charybdotoxin) or synthesized ball peptides (as in the ball-and-chain mechanism) block heterologously expressed K^{+} channels. Accordingly, we excised outside-out patches from *Xenopus* oocytes expressing a human MCU-EMRE (hME) fusion protein in the cellular membrane. Our previous work (29) has demonstrated that hME exhibits similar electrical properties as the uniporters recorded in mitoplasts (23). At negative voltages, hME conducts inward Ca^{2+} currents that are strongly and reversibly inhibited by Ru360 (Fig. 2*A*). We then perfused $MICU1_{EF}$, which includes 4 mutations (D231A, E242K, D421A, and E432K) to eliminate Ca^{2+} binding to the EF hands to lock MICU1 in Ca^{2+}-free conformations. It has been shown qualitatively that transiently expressed $MICU1_{EF}$ in human embryonic kidney (HEK) cells suppresses mitochondrial Ca^{2+} uptake (30), a result we recapitulate here using quantitative $^{45}Ca^{2+}$ flux (Fig. 2*B*). Strikingly, applying $MICU1_{EF}$ reduces macroscopic hME Ca^{2+} currents by 87 ± 4% (Fig. 2*A*), with a current decay time constant of 42 ± 10 s. Moreover, in recordings wherein single-channel transitions can be observed (Fig. 2*C*), $MICU1_{EF}$ greatly reduces hME open time. (These single channels indeed represent the uniporter, as they are reversibly inhibited by nanomolar levels of Ru360 and exhibit a single-channel conductance consistent with that measured in mitoplasts.) The inhibition is not reversible with a 3 to 5 min wash (Fig. 2 *A* and *C*). These results are consistent with purified $MICU1_{EF}$ forming a highly stable complex with hME to block Ca^{2+} permeation through MCU.

We reasoned that the observed $MICU1_{EF}$ block of MCU Ca^{2+} currents is mediated by the MCU–MICU1 interactions observed in uniporter-complex structures (Fig. 1*B*), because both the Jiang and Long labs obtained the MICU1-occluded uniporter structures by adding purified MICU1 to the MCU-EMRE complex in lipid bilayers (20, 21), analogous to what we did in the electrical recordings. To further relate structure and function, we mutated MICU1's K126 residue (Fig. 1*B*), which contacts MCU's D261 ring to block the pore (20–22). $^{45}Ca^{2+}$ flux shows that K126E abolishes the ability of transiently expressed $MICU1_{EF}$ to inhibit mitochondrial Ca^{2+} uptake in HEK cells (Fig. 2*B*). Moreover, perfusing K126E-$MICU1_{EF}$

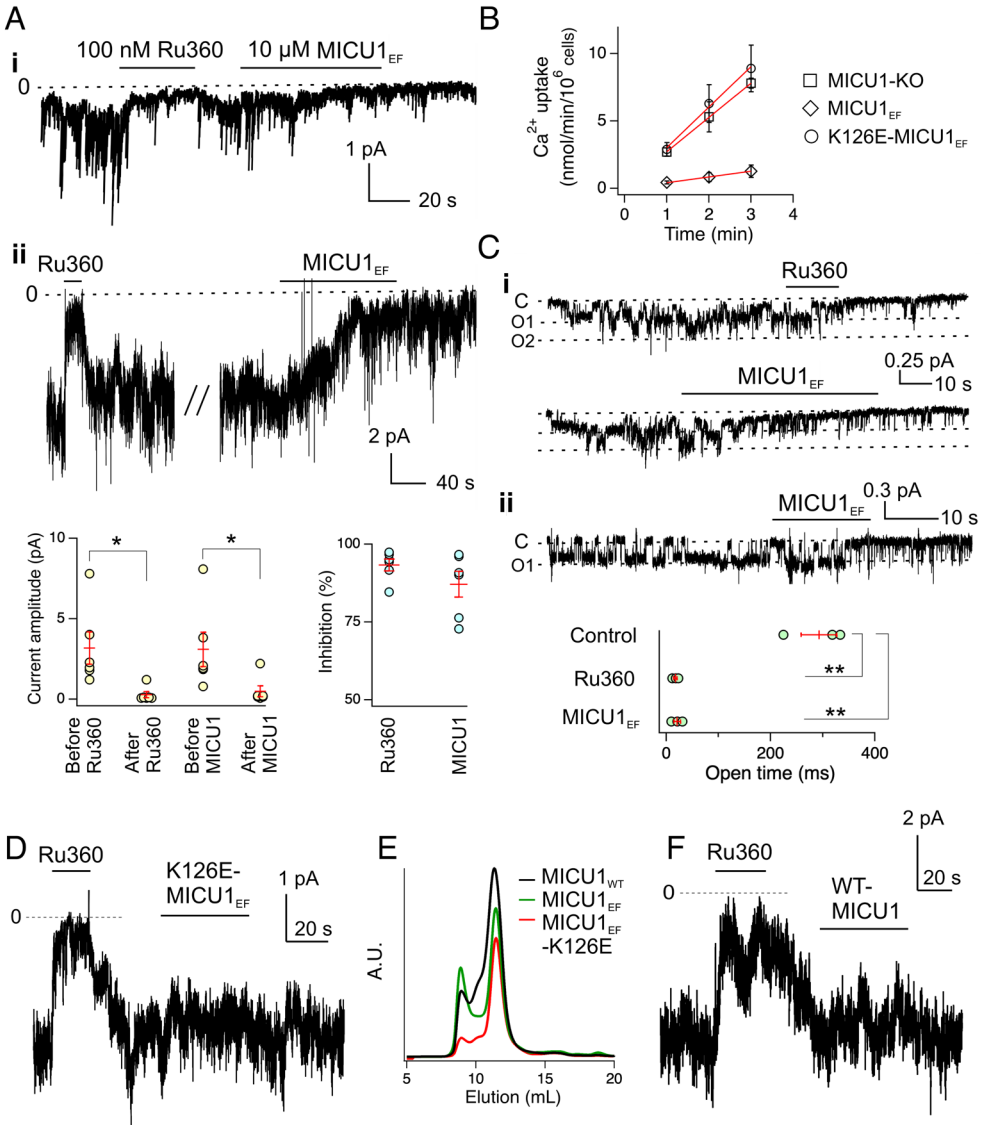

Fig. 2. The effect of $MICU1_{EF}$ on uniporter Ca^{2+} currents. (*A*) The effects of perfusing $MICU1_{EF}$ to patches containing Ca^{2+}-conducting hME. The current amplitude and percentage inhibition by Ru360/MICU1 from each recording are presented along with mean ± SEM in the dot plots. (*B*) Mitochondrial uptake of $^{45}Ca^{2+}$ in MICU1-KO HEK cells. The experiments were performed in the presence of 250 nM Ca^{2+}, with cells transiently expressing indicated MICU1 mutants. N = 5. (*C*) Single-channel recordings showing $MICU1_{EF}$ inhibition of hME. Two continuous traces are shown in *i* and *ii*. Control in the dot plot is the mean channel open time before adding Ru360. (*D*) Mutational effects of K126E on $MICU1_{EF}$ function. N = 3. (*E*) Size-exclusion profiles of WT MICU1 and MICU1 mutants. N = 4. (*F*) Applying WT MICU1 to hME. N = 4. For all electrical recordings in this figure, membrane potentials were clamped at −60 to −100 mV, $MICU1_{EF}$ or WT-MICU1 was tagged with an N-terminal MBP to facilitate proper protein folding in the periplasmic space of *E. coli,* and [MICU1] and [Ru360] are 10 μM and 100 nM, respectively. *P < 0.05; **P < 0.01.

leaves macroscopic Ca^{2+} currents of hME unchanged, indicating that K126E abolishes $MICU1_{EF}$ block (Fig. 2*D*). Size-exclusion chromatography shows that purified K126E-$MICU1_{EF}$ preserves the proper biochemical behavior of $MICU1_{EF}$ (Fig. 2*E*), suggesting that K126E does not perturb MICU1 folding.

To further differentiate the two mechanisms, we perfused WT-MICU1 to Ca^{2+}-conducting hME. The potentiation model predicts that WT-MICU1 would potentiate hME in this high Ca^{2+} condition. By contrast, the occlusion model predicts that WT-MICU1 would pose no effect on hME activity, because the Ca^{2+}-bound form of WT-MICU1 would not block MCU. Fig. 2*F* shows no changes of macroscopic hME currents in response to WT-MICU1. Taken together, our work demonstrates in real time that $MICU1_{EF}$ inhibits MCU via the K126-mediated interaction (Fig. 2 *A*–*E*) observed in the blocked state of the uniporter-complex structure in 0 Ca^{2+} (Fig. 1 *A* and *B*). Moreover, we detected no potentiation of the uniporter by WT MICU1 in high Ca^{2+} (Fig. 2*F*). These results present strong electrophysiological evidence supporting the occlusion mechanism and refute a key concept in the potentiation model that MICU1 does not block.

MICU1 Suppresses Na^+-Induced IMM Depolarization. The potentiation model was also supported by an IMM depolarization assay, in which EDTA is used to chelate divalent cations to induce MCU-mediated Na^+ influx that would depolarize the IMM in intact mitochondria, as can be detected by using tetramethylrhodamine, ethyl ester (TMRE) or methyl ester (TMRM) to follow the dissipation of IMM potentials. Observing comparable IMM depolarization in WT and MICU1-KO cells, Garg et al. (26) argued that MICU1 does not block MCU in 0 Ca^{2+} to prevent Na^+ influx. However, we were puzzled about why mitochondria were suspended in the presence of 1-mM EGTA (26), which would seem to initiate Na^+ influx before applying EDTA. More critically, membrane depolarization was measured

at a single time point: 5 min after EDTA addition (26). Without the kinetic information, it is problematic to draw conclusions about whether MICU1-KO actually affects IMM depolarization.

The potential issues above prompted us to reexamine these depolarization experiments. Accordingly, we permeabilized TMRM-loaded WT or MICU1-KO HEK cells with digitonin, with 2 mM EDTA added in the presence of 5 mM Na^+ to trigger Na^+ influx into mitochondria. To avoid observing off-target effects, we analyzed two independent MICU1-KO lines, one constructed via the transcription activator-like effector nucleases TALEN (transcription activator-like effector nucleases) approach (kindly provided by Vamsi Mootha) and the other by CRISPR/Cas9 (31). Both MICU1-KO lines exhibit much faster IMM depolarization than the corresponding WT cells (Fig. 3 *A* and *B*). Such rapid depolarization is mediated by MCU as it is strongly inhibited by Ru360 (Fig. 3 *B* and *C*). Moreover, IMM depolarization is slow in the presence of 120 mM K^+ (0 Na^+), and can be greatly accelerated by adding 5 mM Na^+ in the same recording (Fig. 3*D*), corroborating the known electrical properties of MCU that it conducts Na^+ much faster than K^+ (32). Taken together, these results demonstrate that MICU1 greatly reduces Na^+ influx via MCU in 0 Ca^{2+}, consistent with MICU1 occluding MCU but arguing against the MICU1 potentiation mechanism.

MICU1 Dissociates from the Uniporter Complex in Mitoplasts. We then sought to understand why MICU1 block of Na^+ currents in 0 Ca^{2+} was not observed in mitoplast patch-clamp recordings (23, 26). As MICU1 contacts the uniporter's TM subunits, MCU and EMRE, via electrostatic interactions (9, 18, 22), it is conceivable that treating and storing mitoplasts in a high-salt buffer (750 mM KCl) (23, 26) might cause MICU1 dissociation from the uniporter complex. Accordingly, we employed quantitative western blot to compare the MICU1/MCU signal ratio in mitochondria and mitoplasts, produced following the procedures in the original mitoplast patch-clamp paper (23). Mitoplasts have a 30% reduction of MICU1/MCU ratio compared with mitochondria (Fig. 4*A*), suggesting that ~30% of MICU1 dissociates into the bulk solution during mitoplast preparation.

Since the uniporter preferentially dwells in areas near the mitochondrial inner/outer membrane contact sites (22), the disruption of such contact sites in mitoplasts could effectively dilute the uniporter in a much bigger surface area, rendering it more difficult for dissociated MICU1 to bind back to the TM region. We thus wonder whether some remaining MICU1 in mitoplasts might only attach to the IMM without being present in the uniporter complex (MICU1 is a peripheral membrane protein). To test this possibility, blue-native PAGE was used to analyze the uniporter complex (Fig. 4*B*). The uniporter in WT mitochondria, detected using an anti-MCU antibody, runs as a smear (lane 3), likely due to the presence of uniporter complexes with different numbers of MICU1. Indeed, the smear is eliminated by MICU1-KO (lanes 5 and 6). MICU1-KO reduces EMRE expression (14, 33), thus creating EMRE-bound (upped band, lanes 5 and 6) and EMRE-free (lower band, lanes 5 and 6) complexes—the latter is also observed in EMRE-KO samples (lane 1). In WT or MICU1-KO mitoplasts, the uniporter runs as a single band without a smear (lanes 4 and 6), thus demonstrating that most MICU1 in the IMM are separated from the uniporter complex after mitoplast production (Fig. 4*C*).

To further assess the functional consequences of MICU1 dissociation in mitoplasts (Fig. 4*C*), we analyzed $^{45}Ca^{2+}$ flux into mitochondria or mitoplasts in 250 nM Ca^{2+} (close to resting cellular [Ca^{2+}]). MICU1-free mitochondria take up much more Ca^{2+} than

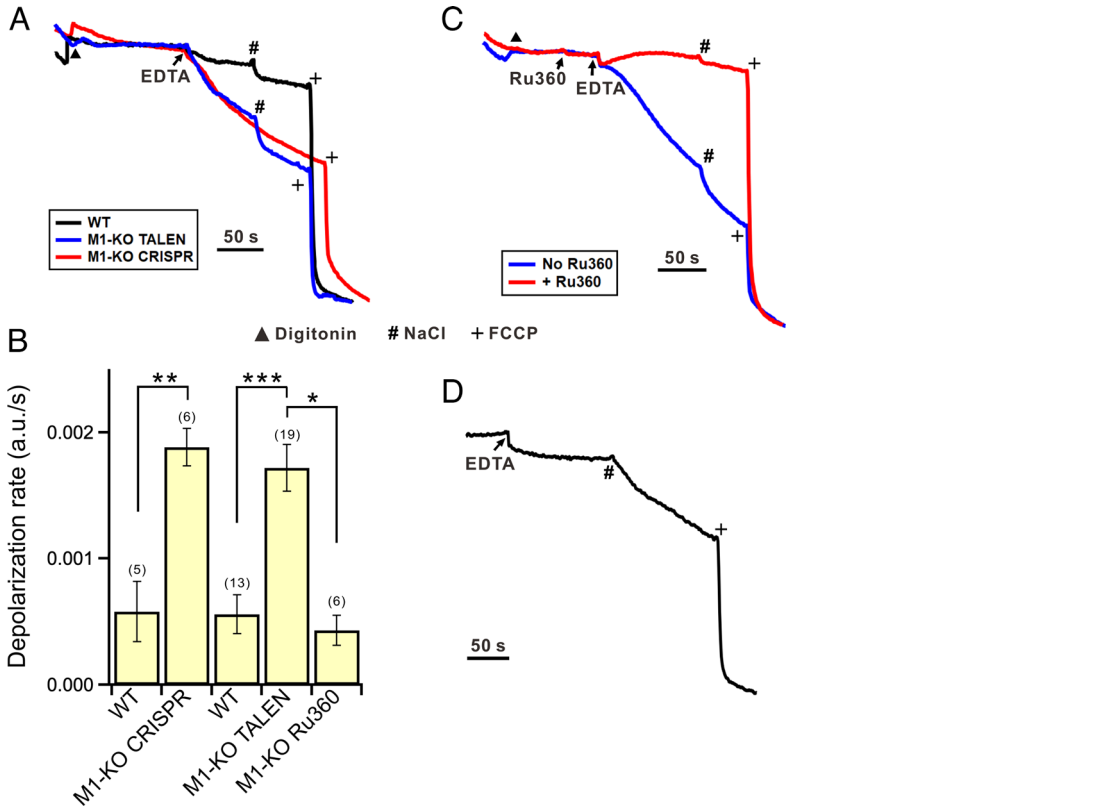

Fig. 3. Suppression of IMM depolarization by MICU1. (*A*) Na^+-induced IMM depolarization in WT versus MICU1-KO cells. EDTA was added in the presence of 5 mM Na^+. In some experiments, another 5 mM Na^+ (#) was added to confirm that the rate of IMM depolarization is saturated with 5 mM Na^+. FCCP was added at the end of the recording to fully collapse the IMM potential. (*B*) A summary of IMM depolarization rates. *M1-KO*: MICU1-KO. (*$P < 0.05$; **$P < 0.01$; ***$P < 0.001$.) (*C*) Ru360 inhibition of IMM depolarization. EDTA was added to permeabilized MICU1-KO cells with or without Ru360 pretreatments. (*D*) IMM depolarization by K^+ versus Na^+. EDTA was added to permeabilized MICU1-KO cells suspended in a Na^+-free buffer that contains 120 mM K^+. N = 5.

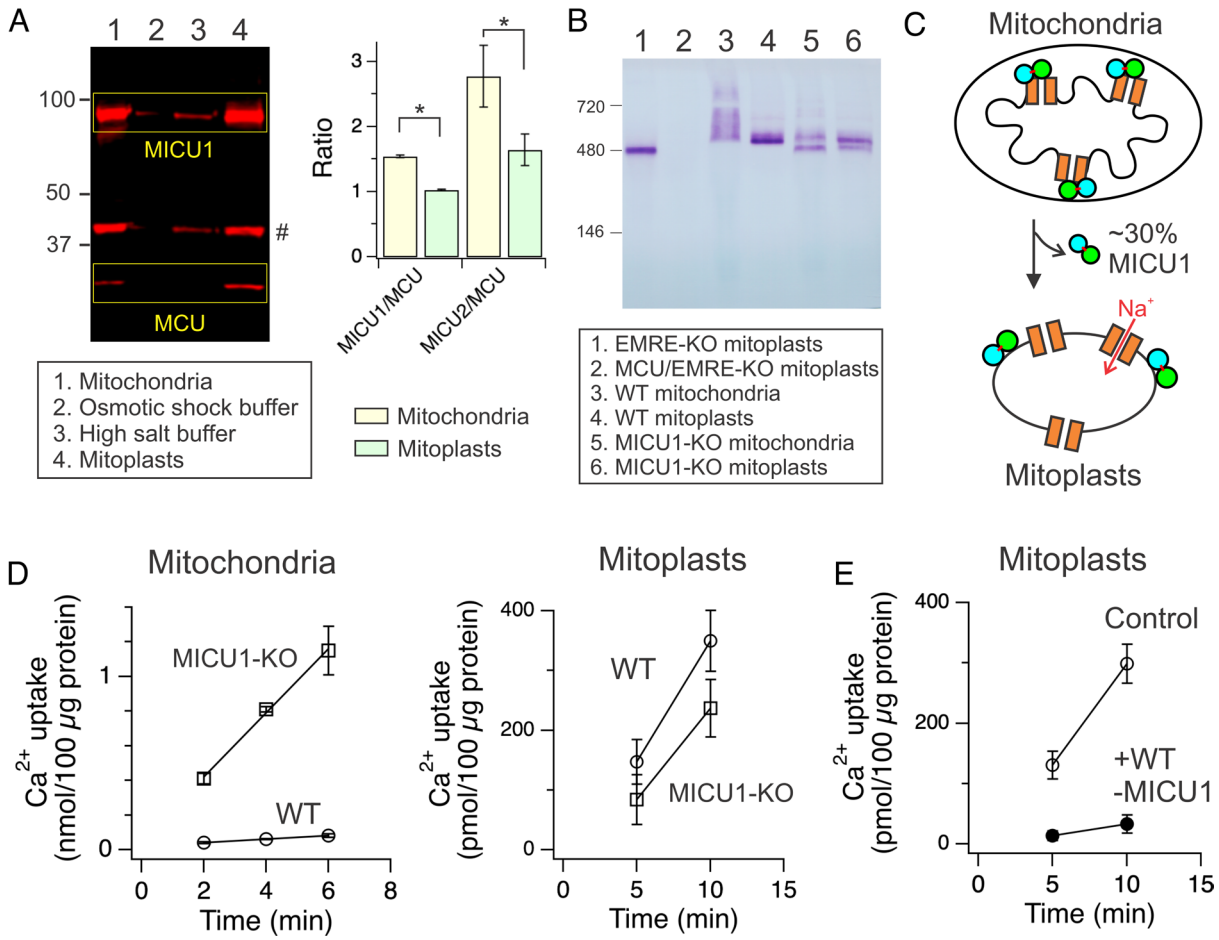

Fig. 4. Biochemical and functional characterization of the uniporter in mitoplasts. (*A*) Changes of the MICU/MCU ratio during mitoplast preparation. The western image shows that MICU1, but not MCU, dissociates into the osmotic-shock and high-salt buffers during the mitoplast production process. The # sign marks a nonspecific band N = 4 to 6. (*B*) BN-PAGE analysis of the uniporter complex. N = 4. (*C*) A cartoon explaining why Na^+ can permeate MCU in mitoplasts in 0 Ca^{2+}. The connected green-cyan balls represent the MICU1–MICU2 heterodimer connected by an intersubunit disulfide. (*D*) Uniporter deregulation in mitoplasts. The experiments were performed in the presence or absence of Ru360 to allow the calculation of uniporter-mediated, Ru360-sensitive Ca^{2+} uptake in mitochondria or mitoplasts. N = 4 to 6. (*E*) Rescue of MICU1 block in mitoplasts. WT mitoplasts were resuspended in a 1-mL wash buffer in the absence (control) or presence of 10-μM WT-MICU1 for 10 min before being spun down and resuspended in a recording buffer for $^{45}Ca^{2+}$ flux (*Materials and Methods*). N = 4.

WT mitochondria (Fig. 4*D*), because the former does not have MICU1 to shut the uniporter under this low-Ca^{2+} condition. Consistent with mitoplasts losing MICU1 from the uniporter complex, WT and MICU1-free mitoplasts show no difference in the rates of Ca^{2+} uptake (Fig. 4*D*). Moreover, incubating WT mitoplasts with 10 μM of purified WT-MICU1 strongly restores MICU1 block of the uniporter in 250 nM Ca^{2+} (Fig. 4*E*). In conclusion, our results demonstrate that mitoplasts possess a population of MICU1-free uniports that remain open to conduct ions even in 0 Ca^{2+}.

MICU1 Does Not Potentiate MCU. MICU1 was proposed to potentiate MCU in elevated [Ca^{2+}] because mitoplast patch-clamp shows that MICU1-KO reduces uniporter Ca^{2+} currents by ~50% in mouse embryonic fibroblast (MEF) cells (26). Indeed, we also reported previously (14) that in >1 μM [Ca^{2+}], MICU1-KO reduces the rate of mitochondrial $^{45}Ca^{2+}$ uptake in HEK cells by ~50%. (When [Ca^{2+}] is <1 μM, mitochondrial Ca^{2+} uptake is faster in MICU1-KO than that in WT cells (14), because in such low Ca^{2+} conditions, MICU1 greatly reduces the uniporter's P_o in WT cells.) This phenomenon does not suggest that MICU1 has a potential function but is caused by lower EMRE in MICU1-KO cells, as rescuing EMRE expression fully restores uniporter activities to WT levels (14). However, when expressing EMRE in MICU1-KO MEF cells, Garg et al. observed no increase of uniporter Ca^{2+} currents in mitoplast patch-clamp (26). To better understand this discrepancy, we requested the same MEF cells and *EMRE*-containing lentivirus vector used in Garg et al. (26). (EMRE-overexpressing MICU1-KO MEF cells were also requested, but these have become unavailable.) In agreement with their data, we found that MICU1-KO MEF cells lose >70% of EMRE and exhibit ~50% slower mitochondrial Ca^{2+} uptake in 10-μM Ca^{2+} compared with WT MEF cells (Fig. 5 *A* and *B*). For unknown reasons, lentivirus produced using the transfer plasmids in Garg et al. (26) or our previous work (31) only marginally increases EMRE in MICU1-KO MEF cells (Fig. 5*A* and *SI Appendix*, *text*), which could explain why these viruses fail to enhance uniporter Ca^{2+} transport both in our hands (Fig. 5*B*) and in the study by Garg et al. (26).

If EMRE level cannot be increased more substantially, how could we possibly test whether the slower mitochondrial Ca^{2+} uptake in MICU1-KO MEF cells is due to reduced EMRE or because MICU1 has a potentiation function? Our answer is to express a mouse MCU-EMRE fusion construct (mME) to impose an obligatory 1:1 MCU:EMRE ratio. Moreover, a D261A mutation was introduced to mME to confer Ru360 resistance (18) so that Ru360 can be applied to selectively inhibit native uniporters in MEF cells, allowing specific measurements of mME activity. No difference of Ca^{2+} transport by D261A-mME

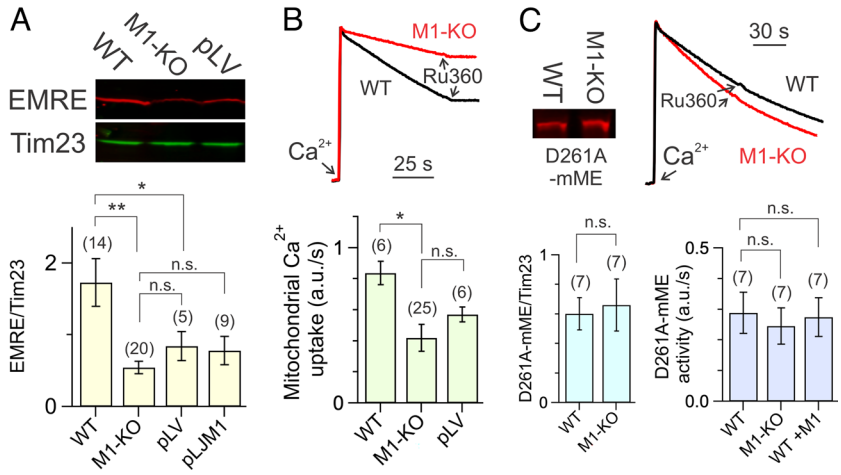

Fig. 5. The effect of MICU1-KO on EMRE expression and uniporter function. (*A*) EMRE reduction and rescue in MICU1-KO MEF cells. *M1-KO*: MICU1-KO. Tim23: loading control. Lentivirus, prepared using the *EMRE*-carrying plasmids in the study by Garg et al. (pLV) or our previous work (pLJM1), were employed to enhance EMRE expression. (*B*) Reduced mitochondrial Ca^{2+} uptake following MICU1-KO. MEF cells were permeabilized in the presence of a Ca^{2+} indicator calcium-green 5N (CG5N), and were subsequently treated with a bolus of 10 μM Ca^{2+}, which increases CG5N fluorescence immediately. CG5N fluorescence then reduces slowly while the uniporter sequesters extramitochondrial Ca^{2+}, until Ru360 was added to inhibit the uniporter. The rate of CG5N signal decline, as summarized in the bar chart, reports uniporter activities. (*C*) The effect of forcing balanced MCU and EMRE expression. The western image and the bottom-left bar chart show that D261A-mME was expressed to similar levels in WT and M1-KO MEF cells. To assess D261A-mME function, permeabilized cells were pretreated with Ru360 to inhibit native uniporters before 10-μM Ca^{2+} was added. *WT+M1*: WT MEF cells transiently expressing both D261A-mME and mouse MICU1. *$P < 0.05$; **$P < 0.01$; *ns*: no statistical significance.

was observed in WT versus MICU1-KO MEF cells in 10 μM Ca^{2+} (Fig. 5*C*), suggesting that MICU1 does not enhance uniporter function. To ensure adequate copies of MICU1 to complex with D261A-mME, mouse MICU1 was coexpressed with D261A-mME in WT MEF cells, but uniporter activities were unaltered (Fig. 5*C*). Taken together, these results with MEF cells, along with our previous work using HEK cells (14), demonstrate that MICU1 has no potentiation function, and that MICU1-KO reduces uniporter transport function in high Ca^{2+} because EMRE, whose binding to MCU is necessary for MCU to transport, is down-regulated.

Discussion

This study provides electrophysiological and biochemical evidence (Figs. 2 and 3) supporting the MICU1 occlusion mechanism and offers alternative interpretations (Figs. 4 and 5) of the results underlying the MICU1 potentiation model. Here, we further examine the two models through the lens of evolution. It is known that the uniporter complex emerges in eukaryotic evolution with only MCU and MICU1 subunits (34), suggesting that MICU1 must regulate MCU through direct physical contacts. Indeed, the MCU–MICU1 interaction is so conserved that human MICU1 can complex with MCU homologs in *Arabidopsis thaliana* (plant), *Dictyostelium discoideum* (amoeba) (18), or *Tribolium castaneum* (beetle) (21). When MCU structures were first determined (1–4), its small and flat IMS surface raises the possibility that docking of MICU1 onto this surface could perturb ion permeation through the Ca^{2+} pore. This is indeed confirmed by subsequent biochemical and structural work (18, 22), leading to the establishment of the occlusion mechanism (Fig. 1*A*). Of note, key residues at the MCU–MICU1 interface (e.g., Y114, Y121, K126, and R129 in human MICU1 and Y258, S259, D261, and I262 in human MCU), as revealed by the structures (20–22), are highly conserved among eukaryotes (22), again highlighting the importance of the MCU–MICU1 contact that blocks the uniporter. In the potentiation model, perhaps realizing that MICU1 would not enhance uniporter activity by binding to MCU's IMS surface, it was speculated that MICU1 potentiates MCU allosterically through EMRE (Fig. 1*C*) (26). Such an argument lacks structural basis, as the MCU-pore conformation appears identical in low and high Ca^{2+} conditions in uniporter holocomplex structures (20–22). Moreover, EMRE is only present in animals (10); if MICU1 function is indeed EMRE dependent, it would problematically imply that MICU1, which coevolves with MCU since early eukaryotes (34), has no function in EMRE-lacking, nonmetazoan organisms.

In mitoplast patch-clamp experiments, Ca^{2+} (I_{Ca}) and Na^{+} (I_{Na}) currents were measured in the same mitoplast to obtain the I_{Ca}/I_{Na} ratio, and MICU1-KO was shown to reduce I_{Ca}/I_{Na} (26). Accordingly, it was argued that MICU1-KO reduces uniporter activities not due to reduced EMRE, as I_{Ca}/I_{Na} is independent of EMRE expression. However, Fig. 6 shows that when EMRE is reduced in MICU1-KO cells (Fig. 5) (26), I_{Ca}/I_{Na} could become lower in MICU1-KO mitoplasts in both occlusion and potentiation mechanisms, so long as WT mitoplasts contain a mixed population of MICU1-bound and MICU1-free uniporters (Fig. 4 *A* and *B*). Thus, I_{Ca}/I_{Na} cannot be used to differentiate the two models. I_{Na}, by contrast, is a more powerful parameter to test the two mechanisms. As illustrated in Fig. 6*B*, the potentiation model requires I_{Na} to be higher in WT than MICU1-KO mitoplasts, because MICU1-KO mitoplasts lose a population of functional uniporter channels due to reduced EMRE. The occlusion model, however, can be consistent with no changes of I_{Na} after MICU1-KO (Fig. 6*A*). Thus, the mitoplast patch-clamp data showing comparable I_{Na} in WT and MICU1-KO conditions (26) are potentially more supportive of the occlusion mechanism. Finally, we note that Garg et al. (26) conducted single-channel recordings showing that MICU1-KO reduces the channel open probability. However, it is unclear whether these single channels represent the uniporter, as no reversible inhibition by ruthenium compounds was shown, and as the channels exhibit quite different electrical properties, including multiple subconductance states and much higher conductance, than those originally described in the Clapham lab (23).

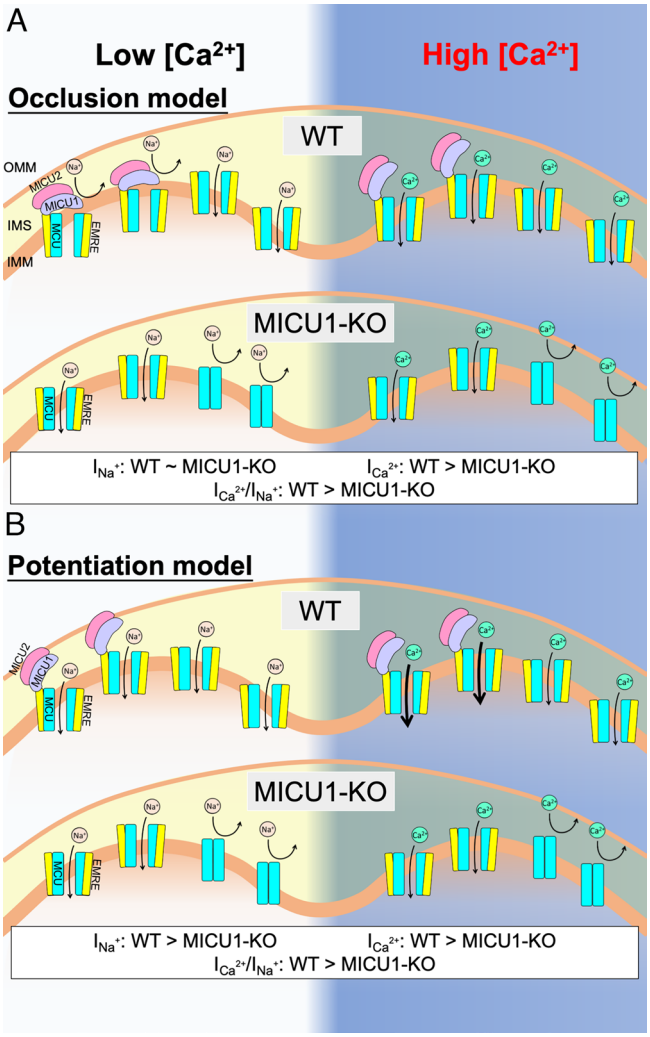

Fig. 6. The predictions of uniporter currents based on the two competing models. (*A*) The occlusion model. (*B*) The potentiation model. Note how the potentiation model demands that the uniporter's Na^+ currents be higher in WT than that in MICU1-free mitoplasts. OMM: outer mitochondrial membrane.

Materials and Methods

Electrophysiology. *Xenopus* oocytes were injected with 60 ng cRNA encoding the human MCU-EMRE fusion protein (hME) and were incubated in an ND96 solution (2 mM KCl, 96 mM NaCl, 1.8 mM $CaCl_2$, 1 mM $MgCl_2$, 5 mM HEPES, pH 7.4-NaOH) at 17 °C as described in our previous work (29). Patch-clamp recordings were performed 3 to 5 d after cRNA injection. Borosilicate pipettes were produced using a Sutter P1000 pipette puller, and were fire polished with a homemade microforge, leading to a pipette resistance of 3 to 5 MΩ. In all experiments, the pipette solution contains 90 mM sodium gluconate, 10 mM NaCl, 5 mM EGTA, 20 HEPES, pH 7.6-NaOH. Outside-out patches were excised from the oocytes in a continuous perfusion ND96 bath, and then moved to the outlet of a fast solution change system (Warner SF-77B) to be perfused with a Ca-100 solution (100 mM $CaCl_2$, 20 mM HEPES, pH 7.6-NaOH). Currents of hME were recorded at room temperature with a HEKA EPC-10 amplifier, filtered at 100 Hz with an eight-pole Bessel filter (Warner), and digitized at a frequency of 500 Hz. The membrane potential was clamped at −60 to −100 mV (more negative voltages were used when the seal was more stable). Negative (inward) currents are defined as currents from the bath to the cytoplasmic side of outside-out membranes. 100 nM Ru360 or 10 μM MICU1 was diluted in Ca-100 and was applied to the patches via the SF-77B fast solution change system.

Protein Purification. DNA encoding N-terminally maltose-binding protein (MBP)-tagged MICU1 proteins were cloned into a pET21b vector. Transformed *Escherichia coli* BL21 cells were inoculated into terrific broth, grown to an OD of 1.0 at 37 °C, and then induced for protein expression by adding 0.1 mM IPTG for 2 h at 37 °C. Cells were pelleted, and resuspended in a breaking buffer (BB, 500 mM NaCl, 25 mM HEPES, pH 7.5-NaOH) supplemented with 1 mg/mL leupeptin/pepstatin and 1 mM PMSF. After lysis by sonication, the lysate was clarified by centrifugation at 16,000 g for 30 min at 4 °C. The lysate wan then loaded onto a cobalt-affinity column. The column was washed and eluted with 10 mM and 200 mM imidazole in BB, respectively. The protein was then concentrated and further purified via a Superdex 200 Increase size-exclusion column equilibrated with BB. Elution volume 10.5 to 12 mL was collected and concentrated down to 150 μM. The concentrated stock was stored at −80 °C and diluted to Ca-100 right before electrophysiological experiments to be used within 4 h. The freeze-thaw process and leaving protein in Ca-100 for 4 h in room temperature does not affect the size-exclusion profiles. The yield of WT-MICU1, $MICU1_{EF}$, and K126E-$MICU1_{EF}$ are 15 mg, 5 mg, and 2.5 mg/L *E. coli,* respectively.

Cell Culture and Molecular Biology. HEK 293 and MEF cells were cultured in Dulbecco's Modified Eagle Medium (DMEM) with 10% FBS in a 5% CO_2 incubator at 37 °C. Deletion of the MICU1 gene in HEK cells was achieved by CRISPR-Cas9 and has been validated previously (31). The genes encoding MICU1 mutants were cloned into a pcDNA3.1(+) vector for transient expression using Lipofectamine 3000 (Life Technologies). Lentivirus to deliver the mouse EMRE gene to MICU1-KO MEF cells was produced using a pLJM1-eGFP vector (Addgene #19319) as described in our previous work (31), or using a pLV-EF1α-IRES-EMRE vector provided by Vivek Garg (26). Transduced MEF cells were treated with 1 μg/mL puromycin for at least four passages (~10 d) before being used for experiments.

Mitochondria and Mitoplast Production. HEK 293 cell mitochondria and mitoplasts were produced following the protocols described in the original mitoplast patch-clamp paper (23) with minor modifications. Briefly, HEK cells suspended in a mitochondrial resuspension buffer (250 mM sucrose, 5 mM HEPES, 1 mM EGTA, pH 7.2-KOH) were disrupted by passing through 27.5 gauge needles 10 to 20 times. Mitochondria were pelleted by differential centrifugation (1,000 g once followed by 13,000 g 3 times) at 4 °C. To obtain mitoplasts, mitochondria were resuspended in an osmotic shock buffer (5 mM sucrose, 5 mM HEPES, 1 mM EGTA, pH 7.2-KOH) for 10 min on ice, spun down at 13,000 g for 10 min at 4 °C, resuspended in a high-salt buffer (750 mM KCl, 100 mM HEPES, 1 mM EGTA, pH 7.2-KOH) for 30 min on ice, and then pelleted by centrifugation at 13,000 g for 10 min at 4 °C. To extract MEF mitochondria, cells were trypsinized and resuspended in an ice-cold isolation buffer (200 mM sucrose, 10 mM Tris, 1 mM EGTA, pH 7.5-MOPS), homogenized using Dounce homogenizers with 25 to 30 strokes, followed by passing through 27.5 gauge needles 50 times. Mitochondria were then separated using differential centrifugation as above.

Western Blot and Blue-Native (BN)-PAGE. To perform western blots, protein samples were subjected to SDS-PAGE and transferred to PVDF membranes. The membranes were treated with primary antibodies at 4 °C for overnight followed by fluorescent secondary antibodies in room temperature for 1 h. The image was acquired using a Li-Cor Odyssey CLx imager. Antibodies and dilutions used in this study: anti-MICU1 (Sigma, HPA034780, 1:5,000); anti-MCU (Cell Signaling, D2Z3B, 1:10,000); anti-1D4 (homemade, 0.1 μg/mL); anti-EMRE (Santa Cruz, 86337, 1:1,000); anti-Tim23 (Santa Cruz, 514463, 1:1,000); IRDye 680RD goat anti-mouse secondary antibody (Li-Cor, 925-68070, 1:15,000); IRDye 680RD goat anti-rabbit (Li-Cor, 925-68071, 1:15,000); and IRDye 800CW goat anti-mouse (Li-Cor, 925-32210, 1:10,000).

BN-PAGE was performed using the Novex NativePAGE Bis-Tris gel system (Life Technologies). 200 μg mitochondria or 45 μg mitoplasts was dissolved in 20 μL NativePAGE buffer supplied with 4% digitonin, 4% glycerol, and 0.5% G-250. Samples were loaded onto 4 to 16% Bis-Tris gels, subjected to electrophoresis at 4 °C, and transferred to PVDF membranes. The membranes were destained by a solution containing 25% methanol and 10% acetic acid, blocked with 5% milk in TBS (140 mM NaCl, 3 mM KCl, 25 mM HEPES, pH 7.4-HCl), and then incubated with anti-MCU antibody (Cell Signaling, D2Z3B, 1:5,000) in TBST (TBS + 0.05% Tween 20) for overnight at 4 °C, followed by anti-rabbit alkaline phosphatase-conjugated secondary antibody (Promega, S3731, 1:5,000 in TBST) at room temperature for 1 h. Colorimetric detection was performed by adding nitro blue tetrazolium/5-bromo-4-chloro-3-indolyl phosphate substrates (Life Technologies) to the membranes.

Mitochondrial and Mitoplast $^{45}Ca^{2+}$ Uptake Assays. To measure mitochondrial uptake of $^{45}Ca^{2+}$, HEK cell mitochondria were isolated using procedures described above and quantified using the bicinchoninic acid assay (Pierce). 350 μg

mitochondria was resuspended in 1 mL wash buffer (WB, 120 mM KCl, 25 mM HEPES, 2 mM KH_2PO_4, 1 mM $MgCl_2$, 1 mM pyruvate, 0.5 mM malate, pH 7.2-KOH), before being pelleted. $^{45}Ca^{2+}$ uptake was initiated by resuspending mitochondria in 350 μL low Ca^{2+} recording buffer (LCRB, 120 mM KCl, 25 mM HEPES, 2 mM KH_2PO_4, 5 mM succinate, 1 mM $MgCl_2$, 0.69 mM EGTA, 0.5 mM $CaCl_2$, 1 mM pyruvate, 0.5 mM malate, pH 7.2-KOH) at 25 °C, terminated at desired time points by adding 100 μL of the suspension into 5 mL ice-cold WB, and filtered through nitrocellulose membranes. The membranes were extracted in a scintillation cocktail for scintillation counting. The rate of mitochondrial Ca^{2+} uptake was obtained by linear fit of data points, with detailed calculation methods provided in our previous work (18). Mitoplast $^{45}Ca^{2+}$ flux was performed in a similar manner, with the following difference: Ca^{2+} uptake was quenched by adding 100 μL mitoplasts to 1 mL ice-cold WB supplemented with 200 nM Ru360 and 5 μM CGP-37157, and external $^{45}Ca^{2+}$ was removed by spinning down mitoplasts at 13,000 g for 10 min at 4 °C. All $^{45}Ca^{2+}$ uptake experiments were performed in the presence or absence of 200 nM Ru360 to allow isolation of uniporter-specific mitochondrial Ca^{2+} uptake.

IMM Depolarization Assay. 2×10^7 WT or MICU1-KO HEK cells were incubated with 40 nM TMRM in Tyrode's solution (130 mM NaCl, 5.4 mM KCl, 1 mM $MgCl_2$, 1 mM $CaCl_2$, 20 mM HEPES, pH 7.8-NaOH) at 37 °C for 30 min, washed using 10 mL Mg^{2+}-free wash buffer (120 mM KCl, 2 mM K_2HPO_4, 50 μM EGTA, 25 mM HEPES, pH 7.2-KOH), and pelleted and resuspended in 2-mL Mg^{2+}-free recording buffer (120 mM KCl, 2 mM K_2HPO_4, 5 mM succinate, 25 mM HEPES, pH 7.6-KOH). The cell suspension was loaded into a stirred quartz cuvette in a Hitachi F-7100 spectrophotometer for recordings at 25 °C (excitation: 573 nm; excitation slit: 5 nm; emission: 590 nm; emission slit: 5 nm; sampling rate: 1 Hz). Cells were permeabilized with 30 μM digitonin (Sigma D141). 2 mM EDTA (with or without 5 mM NaCl) was then added to induce IMM depolarization, followed by using 1 μg/mL FCCP to fully collapse the membrane potential. The rate of IMM depolarization was quantified by normalizing the slope of EDTA-induced TMRM signal decline to the total TMRM signal (the signal difference before adding EDTA and after adding FCCP).

MEF Cell Mitochondrial Ca^{2+} Uptake. 5×10^6 to 2×10^7 MEF cells of MEF cells were washed using 10-mL MEF-flux wash buffer (120 mM KCl, 2 mM K_2HPO_4, 1 mM $MgCl_2$, 50 μM EGTA, 25 mM HEPES, pH 7.2-KOH) and were then suspended in 2-mL MEF-flux recording buffer (120 mM KCl, 2 mM K_2HPO_4, 1 mM $MgCl_2$, 25 mM HEPES, pH 7.2-KOH). The samples were placed in a stirred quartz cuvette and recorded by an F-7100 spectrophotometer (excitation: 508 nm, excitation slit: 2.5 nm; emission: 531 nm; emission slit: 5 nm; sampling rate: 2 Hz) at 25 °C. Reagents were added in the following order: 250 nM calcium green 5N (Thermo C3737), 30 μM digitonin, 10 μM $CaCl_2$, and 75 nM Ru360. For experiments testing D261A-mME function, 150 nM Ru360 was added to inhibit native uniporters before adding $CaCl_2$ to assess D261A-mME activities.

Data Analysis and Statistics. All data points were presented as mean ± SEM. Statistical analysis was performed using two-tailed *t* test, with significance defined as $P < 0.05$. All experiments were done in at least three independent repeats. Analysis of electrophysiological data was performed using Igor Pro 8 (WaveMetrics). Western blot quantification was done using the Li-Cor Image Studio software (version 5.2).

Data, Materials, and Software Availability. Unprocessed western blot and protein-gel images in all figures are available at Mendeley Data (DOI: 10.17632/fv9z323cmy.1) (35). The MICU1 *E. coli* expression vector has been deposited in Addgene (#199180) (36). Cell lines used in this study will be provided upon requests.

ACKNOWLEDGMENTS. We thank Jessica Lee and Dr. Han-I Yeh for technical assistance, Dr. Yuriy Kirichok and Dr. Vivek Garg for providing WT and MICU1-KO MEF cells and constructive discussions during manuscript preparation, Dr. György Hajnóczky for regular communications, and Dr. Christopher Miller for critical reading of the manuscript. This work is supported by the NIH grant R01-GM129345 (to M.T.) and R35-GM137912 (to J.B.).

Author affiliations: [a]Department of Physiology and Biophysics, University of Colorado Anschutz Medical Campus, Aurora, CO 80045; and [b]Dalton Cardiovascular Research Center, University of Missouri, Columbia, MO 65211

1. J. Yoo *et al.*, Cryo-EM structure of a mitochondrial calcium uniporter. *Science* **361**, 506–511 (2018).
2. N. X. Nguyen *et al.*, Cryo-EM structure of a fungal mitochondrial calcium uniporter. *Nature* **559**, 570–574 (2018), 10.1038/s41586-018-0333-6.
3. C. Fan *et al.*, X-ray and cryo-EM structures of the mitochondrial calcium uniporter. *Nature* **559**, 575–579 (2018), 10.1038/s41586-018-0330-9.
4. R. Baradaran, C. Wang, A. F. Siliciano, S. B. Long, Cryo-EM structures of fungal and metazoan mitochondrial calcium uniporters. *Nature* **559**, 580–584 (2018), 10.1038/s41586-018-0331-8.
5. D. De Stefani, A. Raffaello, E. Teardo, I. Szabo, R. Rizzuto, A forty-kilodalton protein of the inner membrane is the mitochondrial calcium uniporter. *Nature* **476**, 336–340 (2011).
6. J. M. Baughman *et al.*, Integrative genomics identifies MCU as an essential component of the mitochondrial calcium uniporter. *Nature* **476**, 341–345 (2011).
7. A. M. Van Keuren *et al.*, Mechanisms of EMRE-dependent MCU opening in the mitochondrial calcium uniporter complex. *Cell Rep.* **33**, 108486 (2020).
8. Y. Wang *et al.*, Structural mechanism of EMRE-dependent gating of the human mitochondrial calcium uniporter. *Cell* **177**, 1252–1261.e13 (2019).
9. M. F. Tsai *et al.*, Dual functions of a small regulatory subunit in the mitochondrial calcium uniporter complex. *Elife* **5**, e15545 (2016).
10. Y. Sancak *et al.*, EMRE is an essential component of the mitochondrial calcium uniporter complex. *Science* **342**, 1379–1382 (2013).
11. M. Plovanich *et al.*, MICU2, a paralog of MICU1, resides within the mitochondrial uniporter complex to regulate calcium handling. *PLoS One* **8**, e55785 (2013).
12. G. Csordas *et al.*, MICU1 controls both the threshold and cooperative activation of the mitochondrial Ca(2)(+) uniporter. *Cell Metab.* **17**, 976–987 (2013).
13. K. Mallilankaraman *et al.*, MICU1 is an essential gatekeeper for MCU-mediated mitochondrial Ca(2+) uptake that regulates cell survival. *Cell* **151**, 630–644 (2012).
14. C. W. Tsai *et al.*, Mechanisms and significance of tissue-specific MICU regulation of the mitochondrial calcium uniporter complex. *Mol. Cell* **82**, 3661–3676.e8 (2022).
15. S. Musa *et al.*, A Middle Eastern founder mutation expands the genotypic and phenotypic spectrum of mitochondrial MICU1 deficiency: A report of 13 patients. *JIMD Rep.* **43**, 79–83 (2019).
16. C. V. Logan *et al.*, Loss-of-function mutations in MICU1 cause a brain and muscle disorder linked to primary alterations in mitochondrial calcium signaling. *Nat. Genet.* **46**, 188–193 (2014).
17. A. N. Antony *et al.*, MICU1 regulation of mitochondrial Ca(2+) uptake dictates survival and tissue regeneration. *Nat. Commun.* **7**, 10955 (2016).
18. C. B. Phillips, C. W. Tsai, M. F. Tsai, The conserved aspartate ring of MCU mediates MICU1 binding and regulation in the mitochondrial calcium uniporter complex. *Elife* **8**, e41112 (2019).
19. M. Paillard *et al.*, MICU1 interacts with the D-ring of the MCU pore to control Its Ca(2+) flux and sensitivity to Ru360. *Mol. Cell* **72**, 778–785.e3 (2018).
20. Y. Wang *et al.*, Structural insights into the Ca(2+)-dependent gating of the human mitochondrial calcium uniporter. *Elife* **9**, e60513 (2020).
21. C. Wang, A. Jacewicz, B. D. Delgado, R. Baradaran, S. B. Long, Structures reveal gatekeeping of the mitochondrial Ca(2+) uniporter by MICU1-MICU2. *Elife* **9**, e59991 (2020).
22. M. Fan *et al.*, Structure and mechanism of the mitochondrial Ca(2+) uniporter holocomplex. *Nature* **582**, 129–133 (2020).
23. Y. Kirichok, G. Krapivinsky, D. E. Clapham, The mitochondrial calcium uniporter is a highly selective ion channel. *Nature* **427**, 360–364 (2004).
24. P. Hess, R. W. Tsien, Mechanism of ion permeation through calcium channels. *Nature* **309**, 453–456 (1984).
25. W. Almers, E. W. McCleskey, Non-selective conductance in calcium channels of frog muscle: Calcium selectivity in a single-file pore. *J. Physiol.* **353**, 585–608 (1984).
26. V. Garg *et al.*, The mechanism of MICU-dependent gating of the mitochondrial Ca(2+) uniporter. *Elife* **10**, e69312 (2021).
27. C. S. Park, C. Miller, Interaction of charybdotoxin with permeant ions inside the pore of a K+ channel. *Neuron* **9**, 307–313 (1992).
28. W. N. Zagotta, T. Hoshi, R. W. Aldrich, Restoration of inactivation in mutants of Shaker potassium channels by a peptide derived from ShB. *Science* **250**, 568–571 (1990).
29. C. W. Tsai, M. F. Tsai, Electrical recordings of the mitochondrial calcium uniporter in Xenopus oocytes. *J. Gen. Physiol.* **150**, 1035–1043 (2018).
30. K. J. Kamer, V. K. Mootha, MICU1 and MICU2 play nonredundant roles in the regulation of the mitochondrial calcium uniporter. *EMBO Rep.* **15**, 299–307 (2014).
31. C. W. Tsai *et al.*, Proteolytic control of the mitochondrial calcium uniporter complex. *Proc. Natl. Acad. Sci. U.S.A.* **114**, 4388–4393 (2017).
32. F. Fieni, S. B. Lee, Y. N. Jan, Y. Kirichok, Activity of the mitochondrial calcium uniporter varies greatly between tissues. *Nat. Commun.* **3**, 1317 (2012).
33. J. C. Liu *et al.*, MICU1 serves as a molecular gatekeeper to prevent in vivo mitochondrial calcium overload. *Cell Rep.* **16**, 1561–1573 (2016).
34. A. A. Pittis *et al.*, Discovery of EMRE in fungi resolves the true evolutionary history of the mitochondrial calcium uniporter. *Nat. Commun.* **11**, 4031 (2020).
35. M.-F. Tsai, Evidence supporting the MICU1 occlusion mechanism and against the potentiation model in the mitochondrial calcium uniporter complex. Tsai et al. Mendeley Data. https://data.mendeley.com/datasets/fv9z323cmy/1. Deposited 30 March 2023.
36. M.-F. Tsai, pET-hMICU1EF. Addgene. https://www.addgene.org/199180/. Deposited 15 March 2023.